

GALEX OBSERVATIONS OF DIFFUSE ULTRAVIOLET EMISSION FROM DRACO

N. V. SUJATHA¹, JAYANT MURTHY¹, RAHUL SURESH², RICHARD CONN HENRY³, AND LUCIANA BIANCHI³

¹ Indian Institute of Astrophysics, Koramangala, Bangalore 560 034, India; sujatha@iiap.res.in, murthy@iiap.res.in

² National Institute of Technology Karnataka, Surathkal, Mangalore 575 025, India; rsbullz@gmail.com

³ Department of Physics and Astronomy, The Johns Hopkins University, Baltimore, MD 21218, USA; rch@pha.jhu.edu, bianchi@pha.jhu.edu

Received 2010 February 9; accepted 2010 September 6; published 2010 October 25

ABSTRACT

We have studied small-scale (2′) spatial variation of the diffuse ultraviolet (UV) radiation using a set of 11 *Galaxy Evolution Explorer* deep observations in the constellation of Draco. We find a good correlation between the observed UV background and the infrared (IR) 100 μm flux, indicating that the dominant contributor of the diffuse background in the field is scattered starlight from the interstellar dust grains. We also find strong evidence of additional emission in the far-ultraviolet (FUV) band which is absent in the near-ultraviolet (NUV) band. This is most likely due to Lyman band emission from molecular hydrogen in a ridge of dust running through the field and to line emissions from species such as C IV (1550 Å) and Si II (1533 Å) in the rest of the field. A strong correlation exists between the FUV/NUV ratio and the FUV intensity in the excess emission regions in the FUV band irrespective of the optical depth of the region. The optical depth increases more rapidly in the UV than the IR and we find that the UV/IR ratio drops off exponentially with increasing IR due to saturation effects in the UV. Using the positional details of *Spitzer* extragalactic objects, we find that the contribution of extragalactic light in the diffuse NUV background is 49 ± 13 photons cm⁻² sr⁻¹ s⁻¹ Å⁻¹ and is 30 ± 10 photons cm⁻² sr⁻¹ s⁻¹ Å⁻¹ in the FUV band.

Key words: dust, extinction – scattering – ultraviolet: ISM

Online-only material: color figures

1. INTRODUCTION

Studies of the diffuse ultraviolet (UV) sky have been an important part of interstellar dust studies over the last four decades (Bowyer 1991; Henry 1991; Murthy 2009) but were limited by the difficulty of observing faint diffuse sources near the limit of the instrumental sensitivity. It has been generally agreed that the low- and mid-latitude diffuse radiation is dominated by the scattering of starlight by interstellar dust but with a baseline at high galactic latitudes, which was variously attributed to either high-latitude dust (Bowyer 1991) or to an extragalactic source (Henry 2002).

Just as the *Infrared Astronomical Satellite* (IRAS) revolutionized the study of the diffuse infrared (IR) emission (Low et al. 1984), data from the *Galaxy Evolution Explorer* (GALEX) have the potential to change our view of the diffuse UV sky. We have begun an ambitious effort to map the diffuse background in all GALEX deep observations (exposure time ≥ 5000 s) with the first of these being observations of a region of nebulosity first observed by Sandage (1976; hereafter “Region I”), later identified as the nearby molecular cloud MBM 30 (Magnani et al. 1985). This region has a comparatively high optical depth in the UV ($0.8 \leq \tau \leq 3.3$) and we found a flat UV emission (Sujatha et al. 2009) despite the IR 100 μm emission increasing by a factor of 2.

In this work, we examine a set of observations of a region in Draco, where the optical depth is much lower ($\tau < 0.5$) but where there is a ridge of dust extending through the field. As with the Region I observations of Sujatha et al. (2009), this field is at high Galactic latitude (33° – 37°) but is about 60° away at a longitude of about 88° . The data are from the GALEX Deep Imaging Survey (DIS), a few of them overlapping with the *Spitzer* First Look Survey (FLS).⁴ Combining these two

studies, we present here the nature of diffuse UV radiation from low optical depth to high optical depth region.

2. OBSERVATION AND DATA ANALYSIS

The GALEX spacecraft was launched in 2003 under NASA’s Small Explorer (SMEX) program with a primary science objective of observing star formation in galaxies at low redshifts (Martin et al. 2005). Light from the sky is collected through a single 50 cm telescope and separated into two bands (far-ultraviolet, FUV: 1350–1750 Å; near-ultraviolet, NUV: 1750–2850 Å) using a dichroic mirror. Independent low noise delay-line detectors record every photon in each band with an overall effective spatial resolution of $5''$ – $7''$ in the sky over a $1^\circ 25'$ field. The data products from the mission include, amongst other files, Flexible Image Transport System (FITS; Wells et al. 1981) images of the FUV and NUV fields and a list of point sources in each field. A complete description of the data processing, the calibration, and the data products may be found in Morrissey et al. (2007).

This work follows our study (Sujatha et al. 2009) on GALEX observations of diffuse emission in Region I and focuses on a set of 11 observations covering an area about 10 deg^2 in the constellation of Draco, with cumulative exposure times of 3000–50,000 s (Table 1). These observations were taken by the GALEX team as part of a program to map the *Space Infrared Telescope Facility* (SIRTF; now the *Spitzer Space Telescope*) First Light locations—hence the target name of “SIRTFFL.” This region (Figure 1) contains the high velocity cloud (HVC) Complex C (Miville-Deschenes et al. 2005) at a distance of more than 800 pc but also, more relevant to our data, the nearby (60 pc) cloud LVC 88+36-2 (Lilienthal et al. 1991), seen as a ridge in the IR emission. This cloud was first discovered to cast a shadow in the X-ray background (Burrows & Meadenhall 1991). Because of the then upcoming *Spitzer* observations, Lockman & Condon (2005) mapped the region in the 21 cm

⁴ See <http://ssc.spitzer.caltech.edu/fls/>

Table 1
Observation Log

Tile Name	R.A. (deg)	Decl. (deg)	l (deg)	b (deg)	NUV Exposure (s)	FUV Exposure ^a (s)	Observation Period (yyyy/mm/dd)	NUV Visits	FUV Visits ^a
SIRTF00-00	259.11	59.91	88.84	35.05	52917.15	52016.95	2003/07/03–2008/08/25	41	39
SIRTF00-01	260.41	59.34	88.08	34.44	26006.10	30922.1	2003/07/04–2004/07/26	20	24
SIRTF00-02	260.09	58.5	87.08	34.66	39037.05	26859.35	2003/08/18–2007/09/02	30	25
SIRTF00-03	258.33	58.86	87.61	35.55	39830.40	29570.9	2003/08/19–2007/09/01	30	28
SIRTF00-04	256.98	59.72	88.76	36.13	3874.45	3874.45	2004/05/01–2004/05/01	3	3
SIRTF00-05	260.68	60.7	89.71	34.2	5305	5305	2004/05/01–2004/05/03	4	4
SIRTF00-06	257.58	60.45	89.6	35.74	27658.75	2540.55	2005/07/25–2008/04/07	22	2
SIRTF00-07	260.54	60.81	89.85	34.26	34376.55	21276.1	2005/07/27–2007/09/02	25	20
SIRTF00-08	262.61	59.15	87.78	33.33	40639.6	22540	2005/06/19–2007/09/01	28	20
SIRTF00-09	257.2	59.72	88.74	36.02	15737.4	2755.45	2005/07/29–2008/04/07	12	2
SIRTF00-10	256.99	58.8	87.63	36.24	27383.75	10757.7	2005/07/25–2007/08/28	21	15
Region I ^b	142.04	70.39	142.3	38.2	35210	14821	2005/01/11–2007/01/04	22	10

Notes.

^a There are often fewer visits in the FUV because of intermittent failures in the FUV power supply.

^b Tile name: G11-005007-J092810p702308.

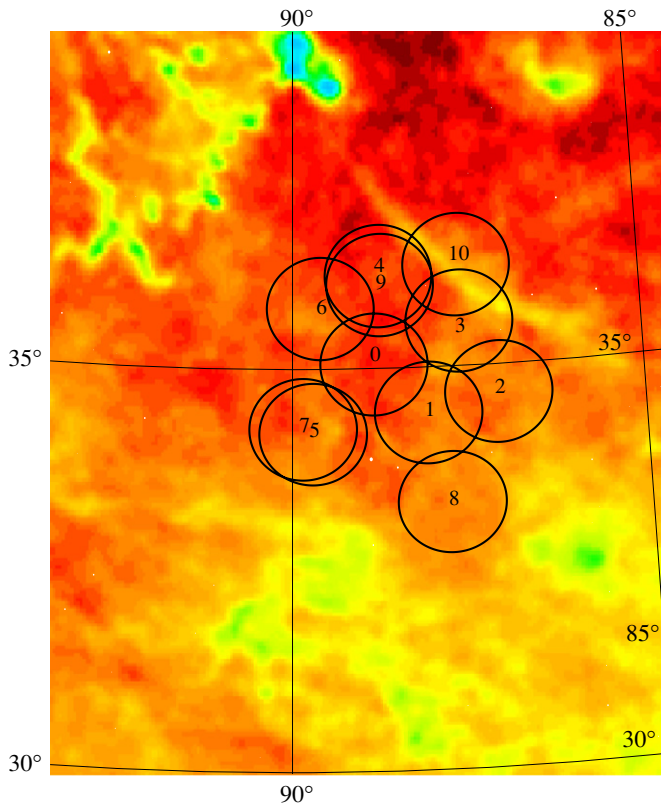


Figure 1. *IRAS* map of the region in galactic coordinates. The *GALEX* field of view of the 11 DIS targets are overlaid as circles with diameter $1^{\circ}25$ and marked as 0–10. The bright arc extending through the fields 3 and 10 is the low velocity cloud (LVC 88+36-2) discussed in the text and the brightest feature on the top left is the Draco Nebula.

(A color version of this figure is available in the online journal.)

line of H I, finding several components (Table 2). This wealth of detail has proven invaluable to our understanding of the UV observations.

Each observation is comprised of a number of visits spread over a period of months, or even years, all of which are coadded by the standard *GALEX* pipeline (Morrissey et al. 2007) to produce a single image in each of the two bands. Point sources in each image were extracted by the *GALEX* team using a standard point source extractor (SExtractor; Bertin & Arnouts 1996) and

Table 2
H I Components in the Field

Cloud	l (deg)	b (deg)	Peak $N(\text{H I})$ (cm^{-2})	V_{LSR} (km s^{-1})
Ridge (LVC)	87.44	35.93	1.8×10^{20}	–2
IVC1	89.47	34.25	5.6×10^{19}	–41
IVC2	88.82	34.17	5.0×10^{19}	–41
IVC3	86.53	33.73	4.4×10^{19}	–34
IVC4 (Draco)	89.85	35.60	7.8×10^{19}	–23
HVC (Complex C)	89.15	35.20	6.9×10^{19}	–190

a merged point-source catalog was created. We note here that the exposure time in the FUV detector was often significantly less than that in the NUV because of intermittent power supply problems. Our processing uses the FITS image files and the merged point-source catalog from the *GALEX* pipeline. These image files have been fully calibrated and flat fielded but not background subtracted. Although the *GALEX* program does provide files containing the background in each observation, these were made by fitting a multi-dimensional surface to the image and therefore show a structure related to the pinning points of the surface. While perhaps adequate for their intended purpose of subtracting the background from point sources in the field, they introduce large-scale artifacts which make them unsuitable for the study of the diffuse radiation field.

Following Sujatha et al. (2009), we created our own background files for each observation by blanking out the point sources in the merged *GALEX* point-source catalog and binning the observation into $2'$ pixels (80×80 *GALEX* pixels). These images form the starting point of our analysis. Because of edge effects, we only used the central $1^{\circ}15$ of the $1^{\circ}25$ field of view for the analysis, rejecting about 20% of the total number of pixels. These background files are comprised of the foreground emission (instrumental dark count, airglow, and zodiacal light) and the astrophysical signal (atomic and molecular emission, dust-scattered starlight, and any extragalactic contribution).

3. FOREGROUND EMISSION

A large field-of-view imager such as *GALEX* has distinct advantages in observations of the diffuse background in that stars can be easily identified and rejected. However, without spectra,

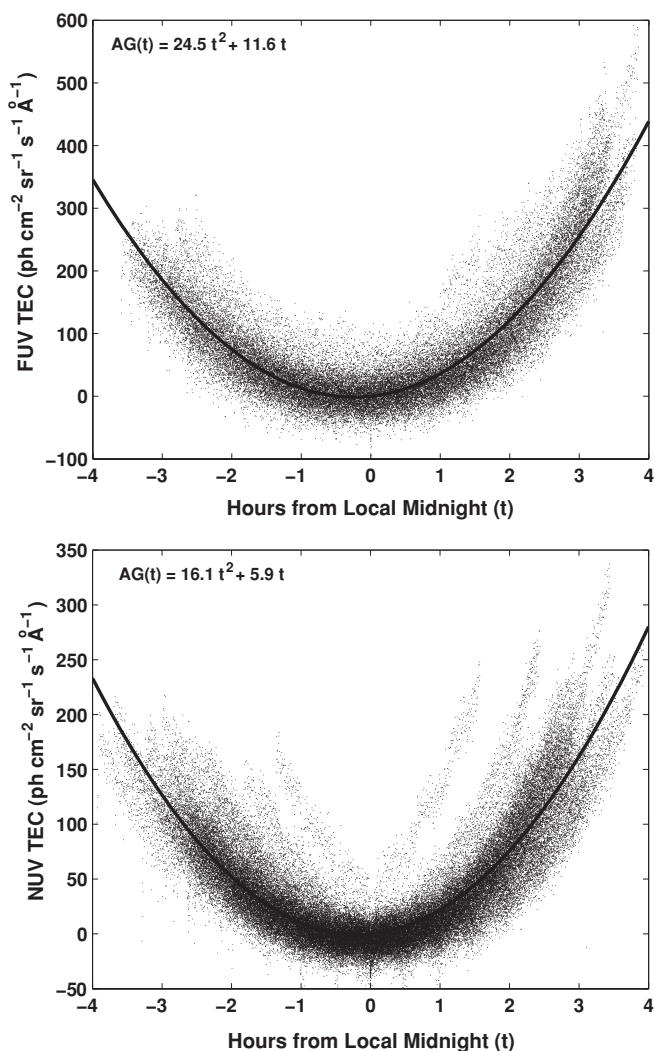


Figure 2. Total count rate (TEC; in photons $\text{cm}^{-2} \text{sr}^{-1} \text{s}^{-1} \text{\AA}^{-1}$) in the FUV (top) and NUV (bottom) is plotted against the local time from midnight. A baseline has been subtracted from each visit so that the count rate is zero at local midnight. The solid line represents the best-fit curve to the data whose quadratic equation is given in the top left of the plot.

we can only infer the contribution of the different components of the diffuse radiation field. Instrumental dark count is negligible, contributing less than 5 photons $\text{cm}^{-2} \text{sr}^{-1} \text{s}^{-1} \text{\AA}^{-1}$ in either band (Morrissey et al. 2007) but airglow, primarily due to the O I lines at 1356 Å and 2471 Å, is expected to contribute about 200 photons $\text{cm}^{-2} \text{sr}^{-1} \text{s}^{-1} \text{\AA}^{-1}$ to either band (Boffi et al. 2007). Although we cannot extract the airglow contribution directly, we have been able to use the Telemetered Event Counter (TEC) of the spacecraft to track the total number of counts as a function of orbital time. Assuming the time-dependent part of TEC present in both the *GALEX* bands as the total foreground emissions, a baseline has been subtracted from each visit so that the count rate is zero at local midnight. The remaining variable component of airglow (AG_v) is well fit with a quadratic as a function of time from local midnight (Figure 2).

In addition, we have found that the baseline levels at local midnight are strongly correlated with the 10.7 cm solar flux⁵ (Figure 3) which is used as a proxy for solar-terrestrial interactions (Chatterjee & Das 1995). Each observation is comprised

Table 3
Airglow and Zodiacal Contribution in Each Field

Tile Name	Average Airglow		Zodiacal Light	Total Foreground Emission ^a	
	FUV	NUV	NUV	FUV	NUV
(photons $\text{cm}^{-2} \text{sr}^{-1} \text{s}^{-1} \text{\AA}^{-1}$)					
SIRTF00-00	391	394	367	396	766
SIRTF00-01	387	338	407	392	750
SIRTF00-02	332	314	373	337	692
SIRTF00-03	318	308	382	323	695
SIRTF00-04	320	378	342	325	725
SIRTF00-05	362	440	342	367	787
SIRTF00-06	306	304	358	311	667
SIRTF00-07	356	313	381	361	699
SIRTF00-08	327	304	365	332	674
SIRTF00-09	333	333	367	338	705
SIRTF00-10	368	369	365	373	739
Region I ^b	349	355	440	354	800

Notes.

^a Includes 5 photons $\text{cm}^{-2} \text{sr}^{-1} \text{s}^{-1} \text{\AA}^{-1}$ dark count.

^b Tile name: G11-005007-J092810p702308.

of several visits, each of which may have a different airglow and zodiacal light contribution. We have estimated and subtracted the zodiacal light from each visit's baseline level and found the y-intercept for each observation, corresponding to stars in the field and the diffuse cosmic background. These values have been subtracted from the individual baseline levels and the resultant values, assumed as the constant airglow (AG_c) in each visit, are plotted in Figure 3. Combining these two results (i.e., $AG_c + AG_v$) allows us to calculate the total airglow (AG) as a function of local time (t ; hours from local midnight) and solar 10.7 cm flux (SF; in 10^4 Jy) with the following equations, with an uncertainty of about 50 photons $\text{cm}^{-2} \text{sr}^{-1} \text{s}^{-1} \text{\AA}^{-1}$:

$$\text{FUV AG} = 3.4 \text{ SF} + 24.5 t^2 + 11.6 t \quad (1)$$

$$\text{NUV AG} = 3.7 \text{ SF} + 16.1 t^2 + 5.9 t. \quad (2)$$

This emission is consistent with an origin of the airglow in solar photons resonantly scattered from geocoronal oxygen atoms. It should, however, be noted that Brune et al. (1978) observed a much lower level of airglow emission with a scaled *GALEX* contribution of about 50 photons $\text{cm}^{-2} \text{sr}^{-1} \text{s}^{-1} \text{\AA}^{-1}$ from their rocket-borne spectroscopic observation. It is possible that some part of what we have euphemistically called “airglow” may be due to some other contributor (Henry et al. 2010).

The remaining foreground contributor, zodiacal light, is important only in the NUV band because of the rapidly fading solar spectrum at wavelengths shorter than 2000 Å. Although there is no UV map of the zodiacal light, we have used the distribution in the visible with gray scattering (Leinert et al. 1998) to predict the zodiacal light in each visit.⁶ The foreground emission (Table 3) ranges from 20% to 50% of the total emission with an uncertainty of about 30 photons $\text{cm}^{-2} \text{sr}^{-1} \text{s}^{-1} \text{\AA}^{-1}$ and estimated using the spatial overlap between different observations. It should be emphasized that the foreground emission affects only the level of the offset and will not affect the spatial variability of the diffuse radiation field.

⁵ <http://www.dxlc.com>, <http://www.spaceweather.ca>

⁶ Calculator at <http://tauvex.iap.res.in/htmls/tools/zodiacal/>

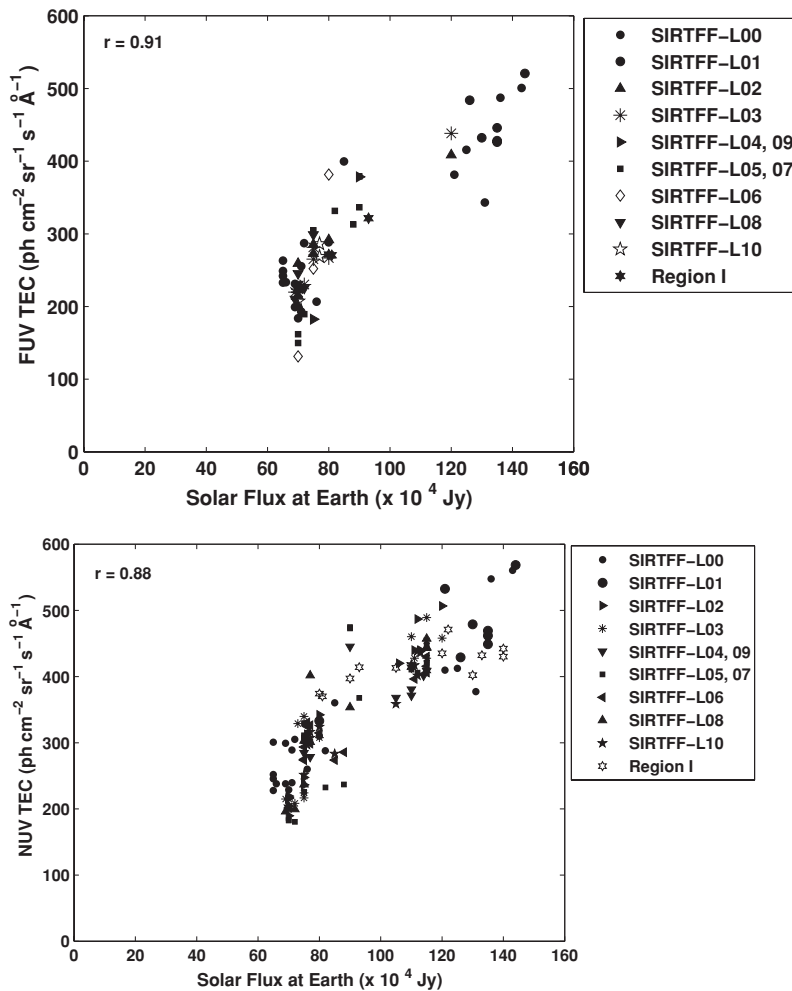


Figure 3. Minimum TEC level in each visit at the local midnight is plotted against the 10.7 cm solar flux at the Earth for FUV (top) and NUV (bottom) channel. An offset was subtracted from each observation (one set of visits). The strong correlation observed here indicates that the variation in the TEC level within an observation is due to solar activity.

3.1. Scatter in the Data

More interesting is the scatter in the data. For a photon-counting instrument such as *GALEX*, the instrumental scatter will be either due to photon noise or to errors in the flat fielding (calibration) of the instrument. We have empirically derived the instrumental scatter by dividing each observation into two sets of visits, which may well be separated by several months. There is excellent agreement between this and the intrinsic photon noise (Figure 4), confirming that the errors are dominated by Poissonian rather than instrumental effects. As an independent test, we also took the overlap regions between different observations and calculated the scatter between them. Although the scatter for the overlap regions is somewhat higher than the calculated values, this is due to the many fewer points in the overlap regions and their location near the edge of the detector. We note here that all our comparisons are in sky coordinates because there are arbitrary roll angle differences between different visits, which do not allow a comparison between physical detector pixels.

4. RESULTS AND DISCUSSION

The FUV and NUV images of the *Spitzer* “First Look” field obtained after subtraction of the foreground emission are shown in Figure 5 at a spatial resolution of 2'. The UV images of

Figure 5 may be compared with the IR 100 μm map (Figure 1). There are several possible contributors to the astrophysical UV emission, a significant one being dust-scattered starlight which contributes to both the FUV and the NUV bands. This is reflected in the good correlation between the FUV and NUV bands (Figure 6) and between the two UV bands and the IR 100 μm fluxes (Figure 7). This is in contrast with the essentially flat UV–IR curves obtained by Sujatha et al. (2009) in Region I. The IR emission is due to thermal radiation from an optically thin layer of dust, as the cross section of the grains is low in the IR. On the other hand, the cross section of the grains is much higher in the UV and the optical depth transitions from being optically thin in these Draco observations to being optically thick in Region I.

In Figure 8, we have plotted the ratio between the UV bands and the IR to understand the nature of diffuse UV emission with optical depth. There is a clear trend visible from the low optical depth Draco region to the high optical depth (in the UV) Region I with an empirical formula of

$$\frac{F_{\text{UV}}}{F_{\text{IR}}} = 415 e^{-0.22 \times F_{\text{IR}}}.$$

It is interesting to note that the $F_{\text{UV}}/F_{\text{IR}}$ ratio in our *GALEX* data follows a continuous curve very similar to that found by Murthy et al. (2001) in Orion using data from the *Midcourse Space*

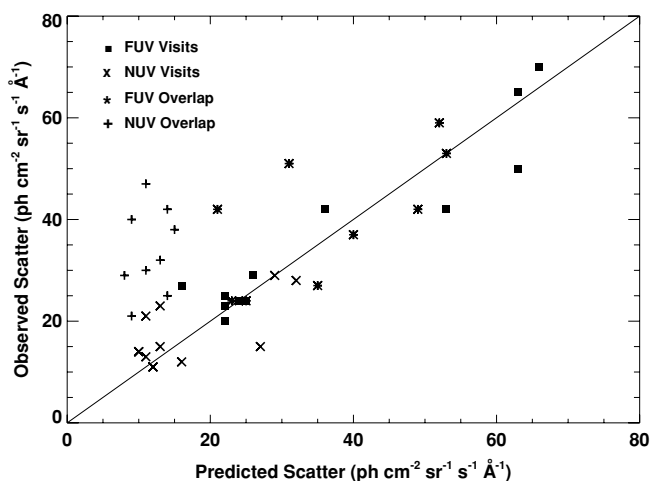


Figure 4. Comparison of observed scatter and intrinsic photon noise in the data. The symbols “filled square” and “x” represent the scatter when a single observation is broken up into two sets of visits for each band, respectively, while the symbols “asterisk” and “+” represent the scatter in the regions of overlap between different observations. In general, the observed scatter is consistent with photon noise alone with the high points being due to the smaller area of overlap.

Experiment (MSX), even though the UV and the IR fluxes in Orion were each greater by a factor of about 200, reflecting the intense radiation field there. However, quite different values are cited in the literature for other regions with ratios ranging from near -50 to almost 260 photons $\text{cm}^{-2} \text{sr}^{-1} \text{s}^{-1} \text{\AA}^{-1}$ (MJy sr^{-1}) $^{-1}$ with little dependence on the IR (Sasseen et al. 1995; Sasseen & Deharveng 1996). It is likely that these relations are only apparent when observed at a high enough spatial resolution; the *MSX* data were at a resolution of $20''$ and our data are at a resolution of $2''$, while the other observations are at resolutions of 0.5 or worse. Since both the IR and the UV vary on smaller scales, the measured $F_{\text{UV}}/F_{\text{IR}}$ ratio may not be a reliable estimator of the true ratio. In fact, Sasseen & Deharveng (1996) found an $F_{\text{UV}}/F_{\text{IR}}$ ratio of 255 photons $\text{cm}^{-2} \text{sr}^{-1} \text{s}^{-1} \text{\AA}^{-1}$ (MJy sr^{-1}) $^{-1}$ for the slope using all their data, higher than any of the individual data sets. In general, we conclude that the $F_{\text{UV}}/F_{\text{IR}}$ ratio in any region strongly depends on the local effects such as the proximity of hot stars near the scattering dust and the optical depth.

Readily apparent in both Figures 7 and 8 is the ridge of dust (LVC 88+36-2) running through our field, where the FUV emission is proportionately greater than the NUV. Indeed, this reflects a general increase in the FUV/NUV ratio with the FUV surface brightness (Figure 9) seen here and in Region I. The most likely explanation for this is that there is an additional component in the FUV band which is not seen in the NUV. Sujatha et al. (2009) suggested that this is fluorescent Lyman band ($1400\text{--}1700 \text{\AA}$) emission of molecular hydrogen, a reasonable assumption in Region I where Martin et al. (1990) had already observed widespread H_2 fluorescent emission.

Assuming that the FUV/NUV ratio for dust scattering alone is constant with a value of 0.8 (Figure 9), we can estimate the level of excess emission in the field. The average error in this ratio, due to the scatter in the data, is estimated to be ± 0.12 . Although the excess emission level in the field is not generally correlated with $N(\text{H I})$ (Figure 10), there is a strong correlation in the ridge (LVC 88+36-2), where the excess emission is likely due to H_2 fluorescence. We obtain a reasonable fit to the data following Martin et al. (1990) and calculate the

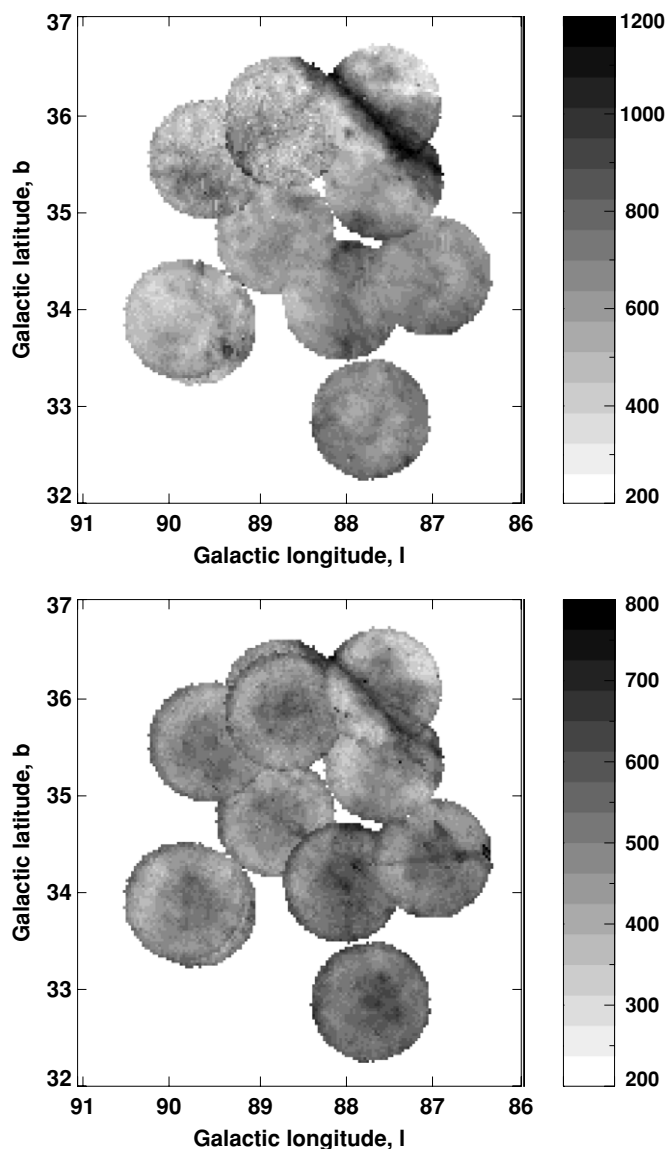


Figure 5. Diffuse FUV (top) and NUV (bottom) images (in photons $\text{cm}^{-2} \text{sr}^{-1} \text{s}^{-1} \text{\AA}^{-1}$) of the region derived from the central $1^\circ 2'$ field of view of each *GALEX* observation. The foreground emission has already been subtracted from each band.

emission assuming a plane-parallel slab with constant density (Figure 11). Park et al. (2009) have observed atomic emission lines of both Si II (1533\AA) and C IV (1550\AA) around the nearby Draco molecular cloud which would effectively contribute about 50 photons $\text{cm}^{-2} \text{sr}^{-1} \text{s}^{-1} \text{\AA}^{-1}$ in the FUV band and it may be that some part of the emission outside the ridge, where there is no correlation with H I , may be due to atomic lines instead.

4.1. Modeling the Dust-scattered Emission

We have applied our standard three-parameter model of interstellar dust scattering (Sujatha et al. 2005) to the continuum dust-scattered light in Draco. This model has been described fully by Sujatha et al. (2005) and uses Kurucz models (Kurucz 1992) for the stars in the *Hipparcos* catalog (Perryman et al. 1997) to calculate the interstellar radiation field (Sujatha et al. 2004). This radiation is then scattered from dust in the line of sight, taking into account self-extinction. The scattering function is from Henyey & Greenstein (1941) and depends

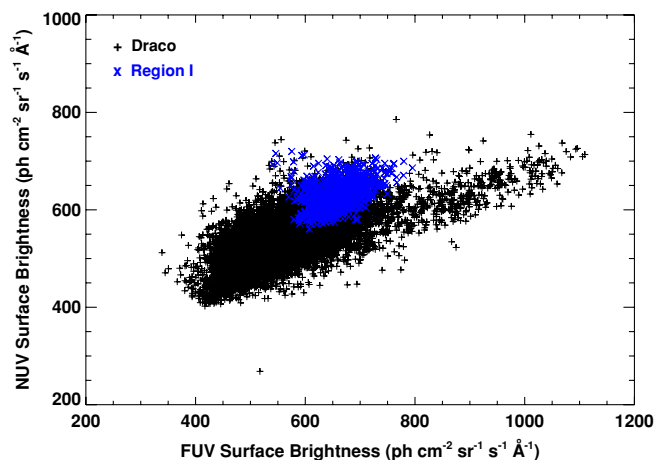


Figure 6. Correlation between FUV and NUV intensity. The blue points (“x”) represent Region I and the black points “+” represent the Draco region. Good correlation between the FUV and NUV bands indicate that the dominant contributor of the diffuse background in the field is scattered starlight from the interstellar dust grains.

(A color version of this figure is available in the online journal.)

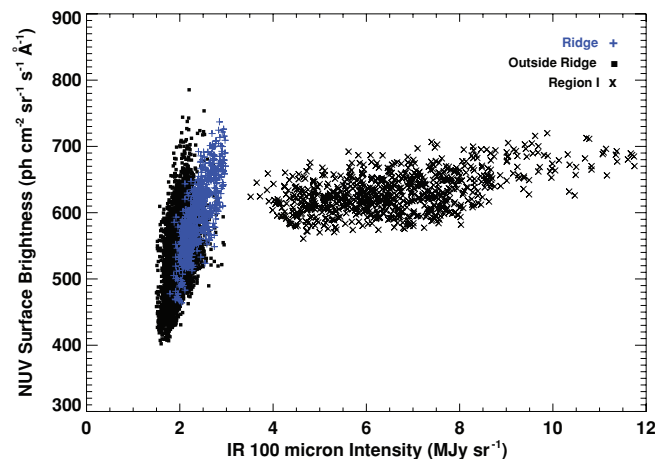
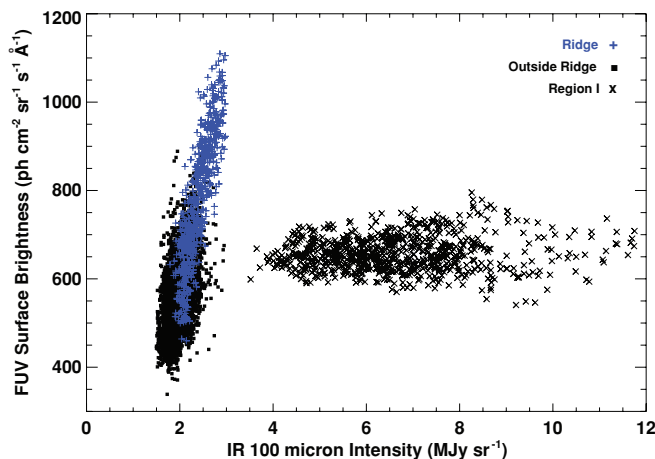


Figure 7. Correlation between *IRAS* 100 μm intensity and diffuse FUV (top) and NUV (bottom) background radiation. In each plot, the blue points (“+”) represent the ridge of dust, the “dots” represent the region outside the ridge, and the “x” points represent Region I. The background radiation is strongly correlated with IR in the Draco region but is saturated in Region I because of the high optical depth in the UV.

(A color version of this figure is available in the online journal.)

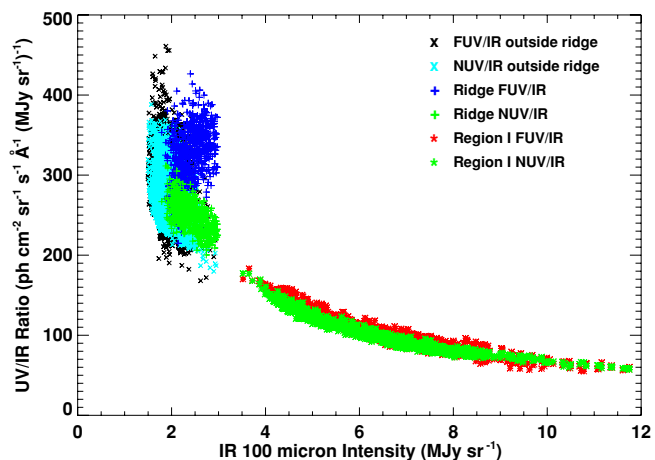


Figure 8. UV/IR ratio (in photons $\text{cm}^{-2} \text{sr}^{-1} \text{\AA}^{-1} (\text{MJy sr}^{-1})^{-1}$) as a function of IR 100 μm intensity. The ratio exponentially drops off with IR due to the rapid increase of optical depth in UV.

(A color version of this figure is available in the online journal.)

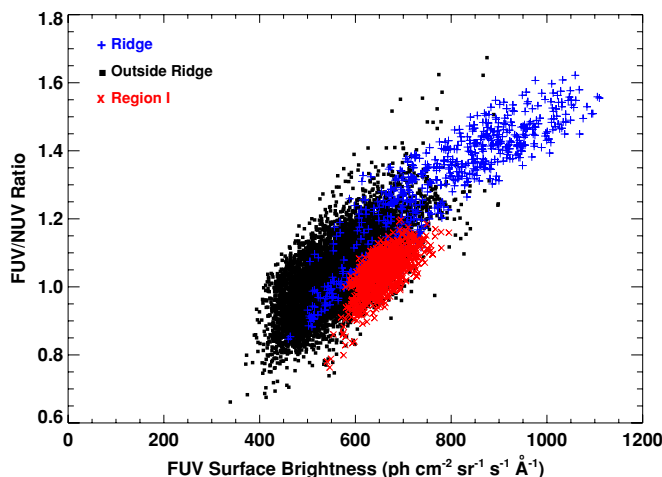


Figure 9. Ratio between the UV bands (after subtracting the foreground emissions) is plotted against the FUV surface brightness. The increase in the ratio with FUV radiation indicates the presence of excess emission in the FUV band.

(A color version of this figure is available in the online journal.)

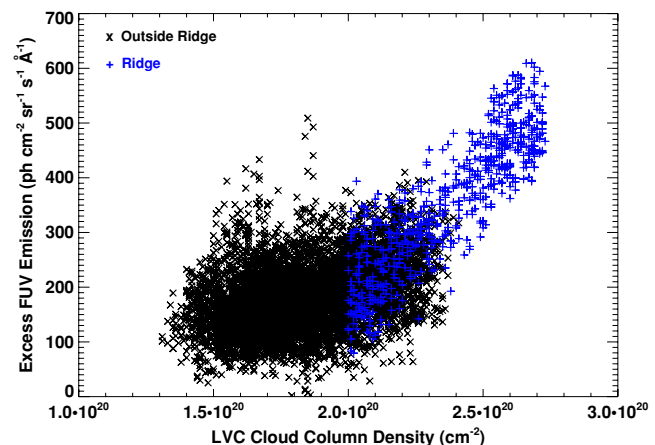


Figure 10. Excess FUV emission in the observations is plotted against $N(\text{H I})$ in the LVC (Lockman & Condon 2005). There is a strong correlation inside the dust ridge where the excess emission is due to molecular hydrogen fluorescence but a poorer correlation outside where the excess emission may be due to line emission from C IV or Si II.

(A color version of this figure is available in the online journal.)

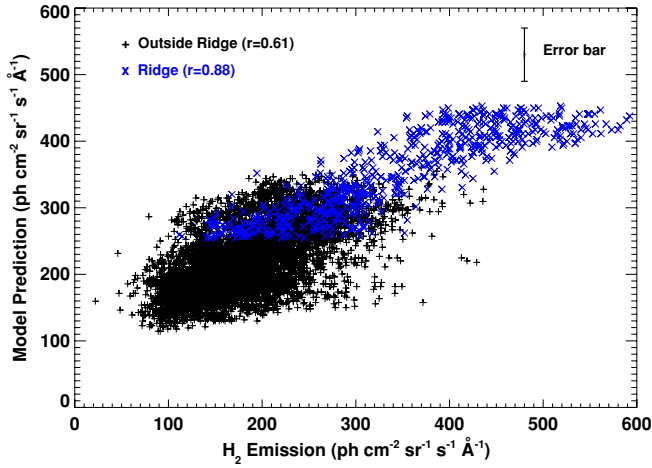


Figure 11. Predicted levels of H₂ emission with a formation rate (R) of $1 \times 10^{-17} \text{ cm}^{-3} \text{ s}^{-1}$ are plotted against the excess emission in the field. There is reasonable agreement everywhere but particularly in the nearby cloud LVC 88+36-2.

(A color version of this figure is available in the online journal.)

Table 4

Correlation Details of UV Emission with Different Components of $N(\text{H I})$

Data	LVC	IVC	HVC	LVC+IVC	LVC+IVC+HVC
FUV Ridge	0.88	0	0	0.84	0.82
FUV Total	0.75	0.3	-0.09	0.70	0.51
NUV Ridge	0.63	0	0	0.63	0.63
NUV Total	0.63	0.27	-0.05	0.63	0.52

only on the albedo (a) and the phase function asymmetry factor ($g = \langle \cos(\theta) \rangle$). Typical values for these suggest moderately reflective ($a = 0.4$), highly forward scattering ($g = 0.6$) grains in the UV, in agreement with the predictions for a mixture of spherical carbonaceous and silicate grains (Draine 2003). Due to the uncertainty of extragalactic contribution (EGL) in the data, we have considered it as a variable parameter in the model. A full treatment of the problem would take into account multiple scattering and clumpiness in the interstellar medium (ISM; see, for example, Gordon 2004) but, because the optical depth is low ($\tau < 0.5$) in our observations, we have used a single scattering model with no clumping. Correlation studies between the UV emissions and different components of H I in the region show that the diffuse emission is maximally correlated with the low velocity cloud (LVC) component of H I, which is the local cloud at 60 pc, and the addition of any other components such as IVC or HVC to LVC reduces the correlation. The details (correlation coefficient, r) are given in Table 4. Hence, for these observations, we have assumed scattering from the local clouds at a distance of 60 pc; very little contribution to the diffuse light comes from the more distant clouds.

With these assumptions, we have placed 1σ limits of 0.45 ± 0.08 on the albedo (a), 0.56 ± 0.10 on g , and $58 \pm 18 \text{ photons cm}^{-2} \text{ sr}^{-1} \text{ s}^{-1} \text{ \AA}^{-1}$ on the EGL in the NUV band with a reduced χ^2 of 1.32. If we use the empirical ratio of 0.8 for the FUV/NUV ratio of the dust, the best-fit NUV values translate into an albedo of 0.32 ± 0.09 and g of 0.51 ± 0.19 in the FUV. These results are in reasonable agreement with previously determined values (Draine 2003). The scatter in our data is more than can be accounted for by photon noise alone. We have empirically derived a 1σ error bar of about 40 photons $\text{cm}^{-2} \text{ sr}^{-1} \text{ s}^{-1} \text{ \AA}^{-1}$ in the model fit to the data compared

Table 5
Number Counts of Extragalactic Objects Present in the NUV Diffuse Map of *Spitzer* Field

AB Mag	N_{objects}	$\text{Log}(N_{\text{objects}} \text{ deg}^{-2} \text{ mag}^{-1})$
20.25	14	0.94
20.75	130	1.91
21.25	584	2.56
21.75	1941	3.08
22.25	3288	3.31
22.75	4211	3.42
23.25	4307	3.43
23.75	3904	3.39
24.25	3364	3.32

to about 20 photons $\text{cm}^{-2} \text{ sr}^{-1} \text{ s}^{-1} \text{ \AA}^{-1}$ from the photon noise, probably reflecting the incompleteness of the model.

4.2. Contribution from Extragalactic Objects

The *Spitzer Space Telescope* (Werner et al. 2004) made its 67 hr FLS near Draco in 2003 in order to characterize the starlight from distant galaxies in the region in mid-IR, using the *Infrared Array Camera* (IRAC; Fazio et al. 2004) and the *Multiband Imaging Photometer for Spitzer* (MIPS; Rieke et al. 2004). The IRAC survey covered an area of 3.8 deg^2 centered on R.A. $17^{\text{h}}18^{\text{m}}00^{\text{s}}$, decl. $+59^{\circ}30'00''$ at wavelengths 3.6, 4.5, 5.8, and $8.0 \mu\text{m}$, with flux density limits of 20, 25, 100, and $100 \mu\text{Jy}$ (Lacy et al. 2005). This instrument produced a band merged catalog of the survey containing 103,193 objects with a positional accuracy of about $0''.25$ for high signal-to-noise objects and about $1''$ at the flux density limits. The overlap area of the IRAC survey is about 38% of the total GALEX observed area in Draco. We have used these important positional details of IRAC cataloged sources to estimate the observed EGL contribution in our diffuse maps. Note that the only expected contribution of EGL in our diffuse maps are from the undetected faint galaxies by SExtractor, since we have removed all the detected sources using the GALEX catalog from each of our field.

We find that some IRAC objects are showing enhancement in the UV intensities from their local background, measured from the $2'$ bin. In Figure 12, the average UV intensities of these objects measured using a diameter of $9''$ (6 pixels) are plotted against the corresponding local background. The UV intensities and the corresponding AB magnitudes of these sources are estimated after subtracting the local background. The total number of such objects detected in the NUV field is 18,989 in the magnitude range 20.0–24.0. The number counts of these objects (Table 5) are shown in Figure 13. By integrating along the curve, we derived the EGL contribution in the NUV map as $49 \pm 13 \text{ photons cm}^{-2} \text{ sr}^{-1} \text{ s}^{-1} \text{ \AA}^{-1}$. The error bar includes both the uncertainties in the magnitude and the area overlapped by IRAC in the field. It is interesting to note that this amount is in good agreement with the extracted value of EGL from the model. We have also found that an accurate estimation of number counts in the FUV band is difficult due to the excess emission in the field and hence we restricted our analysis to the NUV band. However, assuming an average ratio of 0.43 between the FUV and NUV sources derived from Xu et al. (2005) and Hammer et al. (2010) in the magnitude range 20.0–24.0, we estimated the EGL contribution as $30 \pm 10 \text{ photons cm}^{-2} \text{ sr}^{-1} \text{ s}^{-1} \text{ \AA}^{-1}$ in the FUV map from a total of 8165 objects.

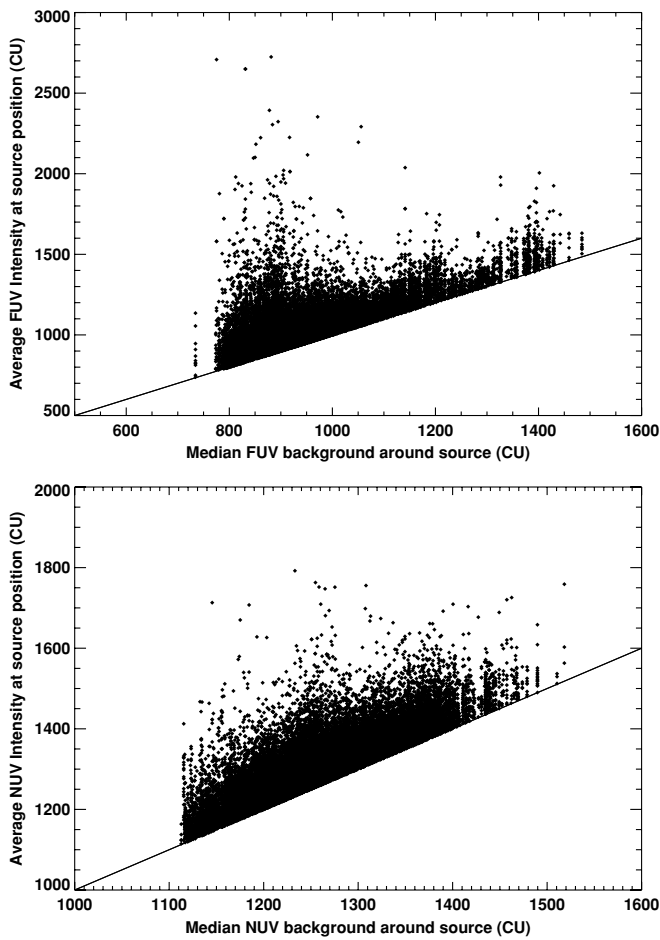


Figure 12. Comparison of average UV intensity (in continuum unit; 1 CU = 1 photons $\text{cm}^{-2} \text{sr}^{-1} \text{s}^{-1} \text{\AA}^{-1}$) from the $9''$ bin and median background from the $2'$ bin centered at each *IRAC* object position in our diffuse maps. The enhancement in some of the *IRAC* source position indicates the presence of undetected faint galaxies by SExtractor in our diffuse maps.

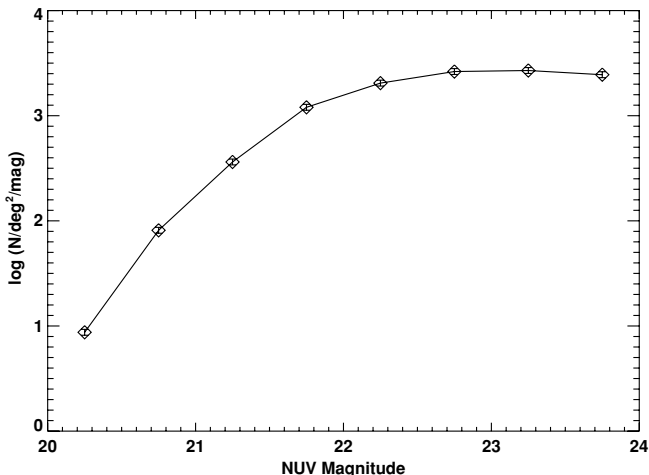


Figure 13. Number counts of extragalactic objects present in the diffuse NUV map of the *Spitzer* field. The solid line is the best-fit curve.

5. CONCLUSIONS

We have completed an analysis of two sets of deep *GALEX* observations: earlier near the Sandage reflection nebula (Region I) toward MBM 30 (Sujatha et al. 2009) and now near the Draco Nebula. In both cases, we have found a good

correlation between the signal in the FUV band (1350–1750 \AA) and the NUV band (1750–2850 \AA) but with an additional component in the FUV which is not seen in the NUV. This was identified as fluorescent emission from the Lyman band of molecular hydrogen in Region I and in the nearby cloud LVC 88+36-2 in these observations, where the ratio was correlated with the H I column density. However, there was excess emission throughout the Draco region which was not correlated (or anti-correlated) with $N(\text{H I})$ and this may be due either to H_2 emission or to line emission from hot gas. While *GALEX* observations are invaluable in probing the diffuse background at unprecedented sensitivity and spatial resolution, spectra will still be necessary to fully understand the observations. However, we strongly recommend that the FUV/NUV ratio can be used to identify the atomic and molecular emission regions in the *GALEX* survey fields all over the sky.

The scattered light from the interstellar dust is consistent with an optically thin layer in the Draco region transitioning to optically thick in the earlier Region I results, although the thermal emission in the IR is optically thin in both cases. The $F_{\text{UV}}/F_{\text{IR}}$ ratio follows an exponential curve across both regions, as would be expected for optically thick media. Interestingly, the $F_{\text{UV}}/F_{\text{IR}}$ ratio in Orion follows exactly the same curve even though both the UV and IR values are higher by a factor of almost 200 due to the intense radiation field. In general, we find that the $F_{\text{UV}}/F_{\text{IR}}$ ratio strongly depends on the local effects such as the proximity of hot stars to the scattering medium and its optical depth.

We have determined optical constants a (0.45 ± 0.08) and g (0.56 ± 0.10) in the NUV band and a (0.32 ± 0.09) and g (0.51 ± 0.19) in the FUV band for the dust in Draco, largely consistent with previous observational and theoretical determinations (Gordon 2004). Regardless of the actual value of the optical constants, we find that the ratio between the FUV and the NUV dust-scattered light is 0.8 over a wide range of optical depths (Draco and Region I). We have also estimated the extragalactic contribution of 58 ± 18 photons $\text{cm}^{-2} \text{sr}^{-1} \text{s}^{-1} \text{\AA}^{-1}$ in the NUV band using our model, which is in good agreement with the derived limit of 49 ± 13 photons $\text{cm}^{-2} \text{sr}^{-1} \text{s}^{-1} \text{\AA}^{-1}$ for the band using the *Spitzer* FLS sources. This gives strong evidence that most of the diffuse background derived from the *GALEX* observations have a Galactic origin specifically at galactic latitudes, $|b| < 40^\circ$.

We have begun a massive program to look at the small-scale structure of diffuse background in all *GALEX* data greater than 5000 s. These include data throughout the sky and sample a variety of different environments, although avoiding bright UV regions such as the Coalsack or Orion. In parallel, we are developing more sophisticated models to better match the high quality data obtained here. We believe the *GALEX* data will allow us to place the study of the diffuse UV radiation on the same level that *IRAS* did for the IR cirrus.

We thank our anonymous referee for the helpful comments and suggestions which have significantly improved this paper. This research is based on data from the NASA's *GALEX* program. *GALEX* is operated for NASA by the California Institute of Technology under NASA contract NAS5-98034. We have also made use of NASA's Astrophysics Data System and the SIMBAD database operated at CDS, Strasbourg, France. We acknowledge the use of NASA's SkyView facility (<http://skyview.gsfc.nasa.gov>) located at NASA Goddard Space Flight Center.

N.V.S. is supported by a DST Young Scientist award. Support for R.C.H. was provided by NASA *GALEX* grant NNGO5GF19G to the Johns Hopkins University.

As always, Patrick Morrissey has greatly helped with our understanding of the *GALEX* data.

Facility: GALEX

REFERENCES

- Bertin, E., & Arnouts, S. 1996, *A&AS*, **117**, 393
- Boffi, F. R., et al. 2007, *ACS Instrumental Handbook*, Version 8.0 (Baltimore, MD: STScI)
- Bowyer, S. 1991, *ARA&A*, **29**, 59
- Brune, W. H., Feldman, P. D., Anderson, R. C., Fastie, W. G., & Henry, R. C. 1978, *Geophys. Res. Lett.*, **5**, 383
- Burrows, D. N., & Meadenhall, J. A. 1991, *Nature*, **351**, 629
- Chatterjee, T. N., & Das, T. K. 1995, *MNRAS*, **274**, 858
- Draine, B. T. 2003, *ARA&A*, **41**, 241
- Fazio, G. G., et al. 2004, *ApJS*, **154**, 10
- Gordon, K. D. 2004, in *ASP Conf. Ser. 309, Astrophysics of Dust*, ed. A. N. Witt, G. C. Clayton, & B. T. Draine (San Francisco, CA: ASP), 77
- Hammer, D., Hornschemeier, A. E., Mobasher, B., Miller, N., Smith, R., Arnouts, S., Milliard, B., & Jenkins, L. 2010, *ApJS*, **190**, 43
- Henry, R. C. 1991, *ARA&A*, **29**, 89
- Henry, R. C. 2002, *ApJ*, **570**, 697
- Henry, R. C., Murthy, J., & Sujatha, N. V. 2010, *BAAS*, **42**, 321
- Henye, L. C., & Greenstein, J. L. 1941, *ApJ*, **93**, 70
- Kurucz, R. L. 1992, in *IAU Symp. 149, The Stellar Populations of Galaxies*, ed. B. Barbuy & A. Renzini (Dordrecht: Kluwer), 225
- Lacy, M., et al. 2005, *ApJS*, **161**, 41
- Leinert, C., et al. 1998, *A&AS*, **127**, 1
- Lilienthal, D., Wennmacher, A., Herbstmeier, U., & Mebold, U. 1991, *A&A*, **250**, 150
- Lockman, F. J., & Condon, J. J. 2005, *AJ*, **129**, 1968
- Low, F. J., et al. 1984, *ApJ*, **278**, L19
- Magnani, L., Blitz, L., & Mundy, L. 1985, *ApJ*, **295**, 402
- Martin, C., Hurwitz, M., & Bowyer, S. 1990, *ApJ*, **354**, 220
- Martin, D. C., et al. 2005, *ApJ*, **619**, L1
- Miville-Deschenes, M. A., Boulanger, F., Reach, W. T., & Crespo, A. N. 2005, *ApJ*, **631**, L57
- Morrissey, P., et al. 2007, *ApJS*, **173**, 682
- Murthy, J. 2009, *Astrophys. Space Sci.*, **320**, 21
- Murthy, J., Henry, R. C., Paxton, L. J., & Price, S. D. 2001, *BASI*, **29**, 563
- Park, S. J., Min, K. W., Seon, K. I., Han, W., Lee, D. H., Edelstein, J., Korpela, E., & Sankrit, R. 2009, *ApJ*, **700**, 155
- Perryman, M. A. C., et al. 1997, *A&A*, **323**, 49
- Rieke, G. H., et al. 2004, *ApJS*, **154**, 25
- Sandage, A. 1976, *AJ*, **81**, 954
- Sasseen, T. P., & Deharveng, J. M. 1996, *ApJ*, **469**, 691
- Sasseen, T. P., Lampton, M., Bowyer, S., & Wu, X. 1995, *ApJ*, **447**, 630
- Sujatha, N. V., Chakraborty, P., Murthy, J., & Henry, R. C. 2004, *BASI*, **32**, 151
- Sujatha, N. V., Murthy, J., Karnataki, A., Henry, R. C., & Bianchi, L. 2009, *ApJ*, **692**, 1333
- Sujatha, N. V., Shalima, P., Murthy, J., & Henry, R. C. 2005, *ApJ*, **633**, 257
- Wells, D. C., Greisen, E. W., & Harten, R. H. 1981, *A&AS*, **44**, 363
- Werner, M. W., et al. 2004, *ApJS*, **154**, 1
- Xu, C. K., et al. 2005, *ApJ*, **619**, L11